

# **Spatially Compact OH Megamasers in Arp 220 and the Nature of the Central Energy Source**

Colin J. Lonsdale<sup>1</sup>, Philip J. Diamond<sup>2</sup>, Harding E. Smith<sup>3,4</sup>,  
and Carol J. Lonsdale<sup>4</sup>

<sup>1</sup>Haystack Observatory, Massachusetts Institute of Technology, Off Route 40, Westford, MA 01886

<sup>2</sup>National Radio Astronomy Observatory, P.O. Box O, Socorro NM 87801

<sup>3</sup>Center for Astrophysics and Space Sciences and Department of Physics, University of California, San Diego, La Jolla, California 92093-0111

<sup>4</sup>Infrared Processing and Analysis Center and Jet Propulsion Laboratory, California Institute of Technology 100-22, Pasadena, CA 91125

## *Summary*

**Arp 220 is the prototypical luminous IR galaxy, and has been the focal point of much debate on the origin, starburst or obscured quasar, of the high luminosity<sup>1</sup> of these objects. It also contains the prototypical OII megamaser source<sup>3</sup>, current models for which involve a low-gain maser screen a few hundred parsecs across, which amplifies background continuum emission from the nuclear regions<sup>4</sup><sup>16</sup>. New line and continuum VLBI observations show that the OII line peak in Arp 220 is dominated by a feature of size <~1 parsec, positionally aligned with a weak continuum VLBI feature. Most of the OII emission from Arp 220 originates on scales < 10 parsecs and reflects a relatively high maser gain, implying physical size scales of the maser regions 10-100 times smaller than previously supposed<sup>5,6</sup>. The maser energetic require a compact, warm, and powerful IR pump source. A plausible model for the maser is that it arises in the dense molecular torus thought to surround many classes of AGN<sup>7</sup>. These results suggest that much of the power output from ultraluminous infrared galaxies may originate in an obscured quasar, not a nuclear starburst.**

The **OII** megamaser phenomenon was discovered<sup>3</sup> in 1982 in the ultraluminous infrared galaxy Arp 220 ( $L_{FIR} \sim 10^{12.1}$ ,  $D = 76$  Mpc with  $H_0 = 75 \text{ km s}^{-1} \text{ Mpc}^{-1}$ ). Megamaser emission is characterized by frequently double-peaked, relatively broad lines, with a high ratio of 1667MHz to 1665MHz line strength<sup>5</sup>. The radio continuum structure of Arp 220 consists of a 1 arcsecond (350pc) double, and each component is barely resolved with ~0.15 arcsec resolution VLA observations<sup>8</sup>. OII line imaging showed that in Arp 220, as in other megamaser galaxies, the line emission has structure which mimics the continuum emission<sup>9,10</sup> which has led to a model in which the emission is due to a foreground screen of unsaturated low-gain ( $\tau \leq 1$ ) masers which amplify intense background continuum emission from the galaxy<sup>4, 5, 6, 11</sup>. Previous VLBI OII observations<sup>11</sup> revealed components of size <30 milliarcseconds associated with each continuum source, which were thought to account for

only 40% of the **single dish** line OH flux. These were interpreted as amplified images of relatively strong, but undetected, inferred V1,III-scale continuum components, consistent with the basic megamaser picture. Radii of 100 to 300 pc for the distance of the clouds from the nucleus are suggested<sup>12</sup>, though a high-velocity outflow may originate from radii as small as 10pc<sup>13</sup>. The powerful 50120 $\mu$ m infrared radiation field of the nuclear region is thought to pump the masers. Among the 50 or so known megamasers, a rough dependence of  $L_{OH} \propto L_{FIR}^2$  has been established<sup>4,5</sup>. The OH gas may trace very high density regions<sup>4</sup> ( $n_{H_2} = 10^{5-7}$ ).

During a continuum global VLBI experiment on September 19 and 20, 1992, data on Arp 220 were obtained using the Effelsberg (100m), Jodrell Bank (76m), Madrid (70111) and Greenbank WV (43m) telescopes. By fortunate chance, the redshifted 1667 MHz OH maser main line fell within the passband of the 28-channel MkIII mode-A observations in a significant subset of these data, allowing us to investigate the properties of the maser at unprecedented angular resolution. Many detections of the maser were made, even on the longest baselines, often with simultaneous detection of continuum fringes. It was, however, possible to achieve high spectral resolution for only a small quantity of data, because most of the original data tapes had been recycled after completion of the continuum-mode correlation.

High resolution spectra for 2 representative baselines/stalls, showing the amplitude and phase of the complex visibility as a function of heliocentric velocity, are presented in Figure 1(a), and (b). The line peak as seen in single-dish observations<sup>3</sup> is dominated by a feature of dimension not exceeding 1 parsec. By integrating the data across all fringe rates and frequencies, we find that roughly 70 percent of the total single dish OH emission occurs on linear size scales of 10pc or less along the line-of-sight to the compact continuum sources. By contrast, the continuum emission is dominated by a diffuse component of linear size  $\sim 100$ pc<sup>8,10,14,15</sup>, and only 1.5 to 3 percent of the flux density is in compact features detected on our VLBI baselines. Each component of the 1-arcsecond double structure in Arp 220

displays the above line and continuum characteristics. Continuum and line fringes from the western nucleus are simultaneously detected in continuum-mode correlations of two, unconfused long baselines. The line and continuum fringe phases on these baselines differ by only 20 and 40 degrees respectively, demonstrating that at least for the western nucleus, the parsec-scale line and continuum features are positionally coincident to within about 0.2pc.

The spectra illustrated in Figure 1, and other spectra in our dataset, demonstrate that the OH line emission is much more physically compact than has been previously supposed. Our VLBI OH line measurements are broadly consistent with previous results<sup>11</sup>, however the fact that we have simultaneous continuum detections allows us to address the question of the location of the maser gas along the line-of-sight to the nuclear continuum sources. This is because we can directly measure amplification factors on various size scales by comparison of simultaneous line and continuum correlated flux densities on various baselines. The maser amplification factor within  $\sim 10$ pc of the VLBI continuum emission is measured to be  $\geq 60$ , and the line emission from these scales accounts for  $> \sim 70\%$  of the single-dish line flux associated with the source. On larger scales, the remaining 30%, combined with  $\geq 97\%$  of the total continuum, yields an average maser amplification factor across the diffuse continuum not exceeding  $\sim 0.3$ . “J’bus, the apparent gain across the source is highly concentrated at sites of VLBI continuum emission, with mean amplification factors increasing by a factor  $\geq 200$  as one moves from the scale of the diffuse continuum (tens to hundreds of parsecs) to below  $\sim 10$ pc scales. Unless our line of sight to this source is highly fortuitous, we must presume that the apparent gain distribution is similar when viewed from all directions, implying that the maser gas is also highly concentrated near the VLBI continuum emission, at each of the two nuclei. The probable physical extent of the bulk of the maser gas is less than 20pc ( $r \leq 10$ pc).

<sup>11</sup> The OH megamaser in Arp 220 thus has a substantially different nature from that previously supposed<sup>5</sup>. Instead of being a large-scale phenomenon produced by molecular

clouds distributed in interstellar space over a volume of order  $10^6 \text{ pc}^3$ , in a region dominated by the nuclear stellar gravitational potential, it is a small-scale phenomenon manifested on scales which imply volumes of  $\leq 10^3 \text{ pc}^3$ , in a region where the gravitational potential is likely to be dominated by a central supermassive black hole.

To assess the FIR pumping photon flux through the maser, a calculation involving the isotropic luminosity of the maser, pump efficiencies, velocity dispersions and other variables is necessary (see e.g. Reid and Moran<sup>16</sup>). We have performed such a calculation under reasonable assumptions (to be reported in detail elsewhere), and find that the maser is probably pumped by a compact, warm ( $r \leq 30 \text{ pc}, T \geq 150 \text{ K}$ ) IR source hidden from direct view by cooler dust which reprocesses the radiation into the observed  $60 - 100 \mu\text{m}$  spectral region on  $> 100 \text{ pc}$  scales. We calculate that an IR source of this size and temperature must supply a fraction  $0.01/\epsilon$  of the total luminosity of Arp 220, where  $\epsilon$  is the pump photon efficiency, in order to power the observed OII emission. Efficiencies above 0.01 are generally thought to be unlikely in discussions of maser pumping. This is a strong constraint on the location of the ultimate power source, and an indication that in Arp 220, much of the luminosity probably originates from a single, central location (i.e. an obscured quasar) rather than from a nuclear starburst distributed over a few hundred parsecs.

The question naturally arises as to the nature of the physical entity which contains the maser gas. Many lines of evidence indicate that the appearance of various classes of AGN is strongly modified by viewing angle<sup>7</sup>, and central to current models for anisotropic radiation is an obscuring dense molecular torus which forms from infalling material in the gravitational potential well of the central supermassive black hole<sup>17</sup>. The physical conditions to be expected within such a torus have been extensively modelled<sup>17,18</sup>, and we can investigate the feasibility of producing the OII maser emission from such a torus.

According to current models, a typical cloud in the torus has number density  $n_H \sim 10^7$ , column density  $\sim 10^{24} \text{ cm}^{-2}$  and temperature  $\sim 10^3 \text{ K}$ . The cloud covering factor to the central AGN source is of order unity. Despite a high ionized fraction ( $\chi_e = n_e/n_H \sim 10^{-3}$ ),

caused by tile penetrating hard X-ray flux from the central source, many of the mode] runs yield clouds transparent to free-free absorption at GHz frequencies. The predicted OH abundances relative to H<sub>2</sub> are typically high,  $\sim 10^{-4}$ , and the far-infrared optical depths are moderate ( $\tau \sim 1$  between 50 and 100  $\mu\text{m}$  for column density  $\sim 10^{24} \text{ cm}^{-2}$ ). In a torus with these properties covering 27r steradians with inner radius  $\sim 3\text{pc}$ ,  $\sim 10^{59}$  OH molecules will be present, sufficient to explain the observed OH luminosity<sup>16,19</sup>.

The observed line profile from a maser torus will depend not only on the gain of the maser gas along various lines of sight, but also on the strength of the background continuum available for amplification along these lines of sight. Since the continuum is sharply peaked, with sub-pc scale features, we should see a strong, relatively narrow line core with weaker broad wings. The Keplerian velocities at a radius of a few pc from a  $1.5 \times 10^7 M_\odot$  black hole (yielding  $5 \times 10^{11} L_\odot$  at the Eddington limit for each of the two nuclei) are close to 200 km s<sup>-1</sup>, so the total velocity width of the wings should be on the order of 400 km S-1. This accurately describes the observed single-dish line profile<sup>3</sup>. As in any model, the narrow linewidths seen at higher resolutions in our data can be attributed to individual maser clouds along a single line of sight.

In summary, an AGN molecular torus model for the OII megamaser in Arp 220 fits the observations remarkably well, and in conjunction with the maser pumping constraint discussed earlier appears to be an attractive working hypothesis. It has been pointed out<sup>18</sup> that the torus itself is a copious source of IR photons, and the outer parts of the torus may well represent the maser pumping source.

Arp 220 is commonly used in litmus tests of AGN versus starburst models of ultraluminous IR galaxies<sup>20</sup>, and as such is regarded as typical of its class 2'. If our results can thus be extended to the general population of megamaser galaxies, observations of the many OII megamasers accessible to VLBI offer a powerful new probe of AGN molecular tori and the hitherto virtually unobservable interiors of the nuclei of highly obscured galaxies. Furthermore, the extensive current data base on the 50 or so known OII megamasers<sup>5</sup> represents

fertile ground for the investigation of torus and host galaxy properties, through analysis of line ratios and profiles in the context of a new interpretation. Our arguments on the pumping energetics would presumably apply to megamaser galaxies in general, strongly favouring an obscured AGN origin for the FIR luminosity.

The established  $L_{OH} \propto L_{FIR}^2$  relationship is consistent with this new picture. Evidence is available that the continuum VLBI-scale radio power  $L_{VLBI}$  is proportional to  $L_{FIR}$  in FIR galaxies<sup>22</sup>. The continuum luminosity on parsec scales available for amplification by OH gas in the torus is  $L_{VLBI}$ , different by a large factor from the continuum luminosity on larger scales used in previous arguments of this type. At the same time, the flux of IR pumping photons is also proportional to the FIR luminosity, so that  $L_{OH} \propto L_{FIR} L_{VLBI} \propto L_{FIR}^2$ , as observed.

Since a torus model predicts only megamaser angular sizes resolvable only with V],]), reports of apparent spatial velocity gradients on larger scales<sup>19,23</sup> would seem to conflict with such a model. However, these galaxies are strongly associated with galactic merger events, and the presence of two nuclei, each with its own masering torus, may be common (compare the early VLA observations<sup>9</sup> of Arp 220). We support the suggestion<sup>6</sup> that the typical double-peaked line profile in OH megamasers is also a consequence of dual nuclei in merging systems, which may be very close together spatially.

Finally, Figure 1 (b) shows evidence for significant emission on the blue side of the main peak, out to  $\sim 5000$  km s<sup>-1</sup>. The flux density in this region is estimated to be  $30 \pm 10$  mJy, which when compared to a single-dish spectrum taken only 4.5 years earlier<sup>13</sup> suggests variability, but we hesitate to interpret it as such because of baseline subtraction and calibration uncertainties in the single-dish data.

## REFERENCES

1. Solomon, P.M. & Sage, L.J. *Astrophys.* 3.334, 613-625 (1988),
2. **Sanders, I.II. eta/., Astrophys .J.325,74-91 (1988).**
3. Baan, W. A., Wood, P.A.D. & Haschick, A.D. *Astrophys.J.* 260, 1,49-1,52 (1982).
4. Baan, W.A. in *Astronomical Society of the Pacific, Conference Series, vol. 16* (eds Haschick, A.J. & Ho, I.'I'.1') 45-56 (1991).
5. Baan, W.A. in *Sub-Arcsecond Radio Astronomy* (eds Davis, R.J. & Booth, R. S.) 324 330 (1 993).
6. Henkel,C.& **Wilson, 'J.]..** *Astron. Astrophys.* 229, 431-440(1990).
7. Antonucci, R. *Ann.Rev.Astr.Astrophys.* 31, 473-521 (1993).
8. Norris, R.P. *Mon.Not.R.Astr.Soc.* 230, 345-351 (1988).
9. Baan, W.A. & Haschick A.J). *Astrophys.J.* 279, .541-549 (1984).
10. Norris, R.] ', Baan, W. A., Haschick, A.J), Diamond,P.J.& BoothR.S. *Mon.Not.R.Astr. Sot.* 213, 821-831 (1985).
11. Diamond,P.J., Norris, IL.] ', Baan,W.A.& Booth, 1{. S. *Astrophys.J.* 340, 1,49-1,52 (19s9).
12. Henkel, C., Gusten, R.& Baan W.A. *Astron. Astrophys. J* 85, 14-24 (J 987).
13. Baan, W. A., Haschick,A.D.& Henkel,C. *Astrophys.J.* 346, 680-689 (1989).
14. Condon, J. J., Huang, Z.-} ', Yin,Q.F.& Thuan, T.X. *Astrophys.J.* 378,65-76 (1991).
15. Lonsdale, C. J., Smith, H.E. & Lonsdale, C.J. *Astrophys.J.* 405, 1,9-1,12 (1993).
16. Reid, M.J. & Moran, J.M. in *Galactic and Extragalactic Radio Astronomy* (eds Verschuur G.L.& Kellermann, K.J. ) 255-294 (Springer-Verlag 1988).
17. Krolik, J. II. & Lepp, S. *Astrophys.J.* 347, 179-185 (1989).
18. Pier, E.A. & Krolik, J.H. *Astrophys.J.* 410, 99- 109 (1 992).
19. Montgomery, A.S. & Cohen, R.J. *Mon.Not.R.Astr.Soc.* 254, 231'-261' (1 992).
20. Solomon, P.M., Radford, S.J.E.&Downes, 1). *Astrophys.J.* 348, 1,53-1,56 (1 990

21. Kormendy, J. & Sanders, D.B. *Astrophys.J.* 390, 1,53-1,56 (1993).
22. Lonsdale, C. J., Smith, H. E. & Lonsdale, C.J. *Astrophys. J.* (submitted).
23. Baan, W.A. & Haschick A. II. *Astrophys. J.* 364, 65-76 (1990).

**ACKNOWLEDGEMENTS** We thank M. Titus and L. Sims for technical assistance, and R. Barvainis, J. Krolik, J. van Buren, M. Reid and J. Moran for valuable discussions and advice. This work was supported at Haystack observatory by the National Science Foundation.

Figure 1. Fringe amplitude and phase as a function of heliocentric velocity, relative to the OH transition at 1667.359 MHz, for two representative baselines. The data analysis, including fringe searching, was performed using the NRAO AIPS software package. In interferometry, weak signals are most easily recognized by a non-random phase distribution; in the displayed spectra weak detections are evident through non-random channel-to-channel phase distributions in several places, despite low amplitudes. Calibration of the visibilities was performed using the gain and system temperature measurements supplied by each observatory. The calibration was refined using continuum observations of barely-reolved extragalactic calibrator sources 1611 + 343 and 0235+164 under the assumption of flat visibility curves on the longer baselines. The calibration accuracy is estimated to be  $\pm 15\%$ .

**Figure 1(a) Emission is** detected in about 20 channels (68 km s $^{-1}$ ). The main peak is only  $\sim 10$  km s $^{-1}$  wide (resolution = 3.4 km s $^{-1}$ ), and accounts for  $\sim 80\%$  of the single-dish flux density at the peak frequency; it is not possible to see this much flux unless the angular size of the component responsible for the fringes on this baseline is less than about half the fringe spacing, or of order 1 pc. Fringes of comparable strength were seen on other baselines with fringe spacings down to 6.0 milliarcsec (2.1 pc).

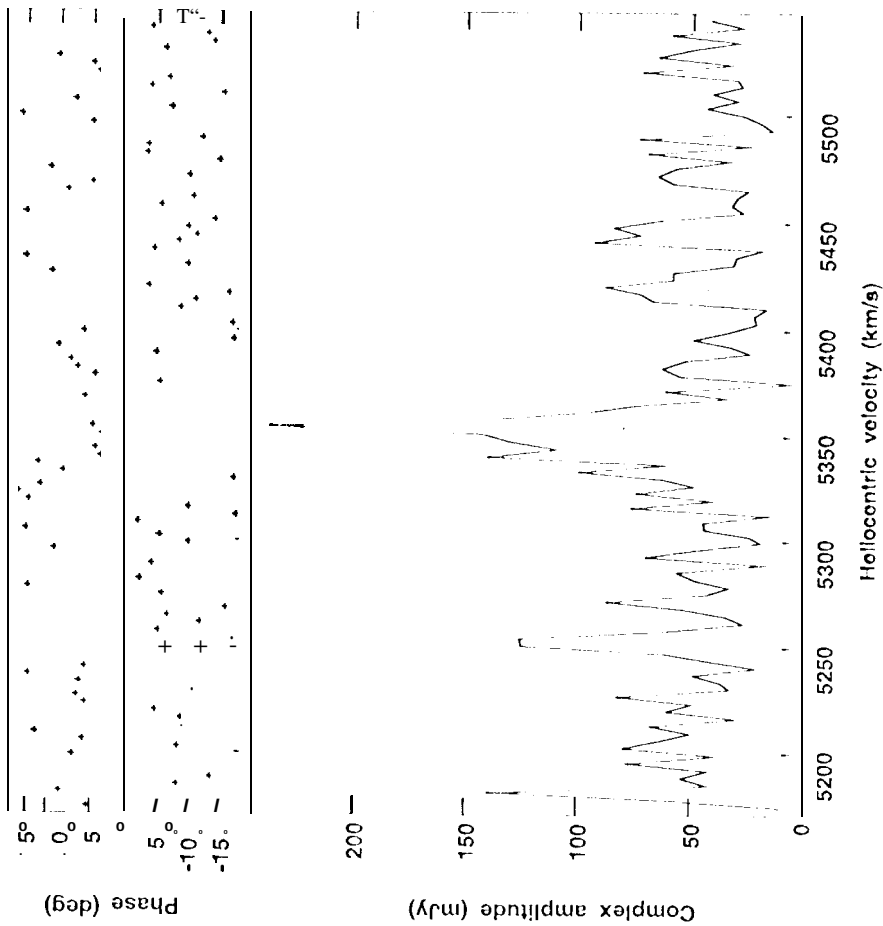
The amplitude of the line peak is 51 times higher than that of simultaneously-detected continuum fringes, a measure of the maser amplification factor. Amplification factors of  $\sim 60$  to  $\sim 80$  are measured on other baselines with a wide range of fringe spacings, and if the line and continuum structures differ significantly, still higher values are implied.

**Figure 1 (b)** A 4 MHz spectrum showing the blue wing to best advantage, with velocity resolution 10.2 km s $^{-1}$ , and a 4-minute integration time to reduce loss of signal due to beating between the two nuclei. The line emission originates from two separate regions roughly 1 arcsecond apart<sup>9,11</sup>, with a separation/size ratio of at least 30. We can account for at least 70% of the single-dish flux density on baselines of this length by performing a coherent integration across all fringe rates and all frequencies. This emission must therefore originate on scales smaller than about 10 pc.

Coherence of the phase distribution indicates that emission is detected over  $\sim$ 450 km s $^{-1}$ , mostly on the blue side of the main peak. The amplitudes suffer from severe noise bias at these signal levels, but from the phase dispersion we deduce a mean correlated flux density between 5000 km s $^{-1}$  and 5200 km s $^{-1}$  of 30±10 mJy, including calibration uncertainty.

The dashed line is the Arecibo single-dish spectrum taken from Baan, Wood and Haschick<sup>3</sup>, presented for comparison purposes. It is intended to illustrate the velocity registration of certain features only, and because of the sharply differing nature of the datasets (one a real quantity, the other a complex quantity with complications due to fringe rate resolution), should not be compared in detail, especially in the line wings. In particular, note that any single slice through our dataset in fringe rate, such as this figure, does not represent the total OH luminosity on these scales, thus a direct comparison with the single-dish flux density is not possible from this figure.

Jodrell - Greenbank (fringe spacing 7.5 milliarcsec = 2.6pc)  
Freq = 1.6370 GHz, Bandwidth = 2 MHz



Eftelöv-Jodrell (fringe spacing 70 milliarcsec = 24pc)

Freq = 1.6370 GHz, Bandwidth = 4 MHz

